Correcting for sparsity and non-independence in glycomic data through a systems biology framework

Bokan Bao[1,2,3,+], Benjamin P. Kellman[1,2,3,+], Austin W.T. Chiang[1,2], Austin K. York[1,2], Mahmoud A. Mohammad[4], Morey W. Haymond[4], Lars Bode[1], Nathan E. Lewis[1,2,5,*]

[1] Department of Pediatrics, University of California, San Diego, La Jolla, CA 92093, USA

[2] The Novo Nordisk Foundation Center for Biosustainability at the University of California, San Diego, La Jolla, CA 92093, USA

[3] Bioinformatics and Systems Biology Graduate Program, University of California, San Diego, La Jolla, CA 92093, USA

[4] Department of Pediatrics, Children's Nutrition Research Center, US Department of Agriculture/Agricultural Research Service, Baylor College of Medicine, Houston, Texas 77030, USA

[5] Department of Bioengineering, University of California, San Diego, La Jolla, CA 92093, USA

[+] These authors contributed equally to this work

[*] Corresponding author:

Name: Nathan E. Lewis

Address: 9500 Gilman Drive MC 0760, La Jolla, CA 92093

E-mail: nlewisres@ucsd.edu

Short running title: Comparative glycoprofile analysis with glycan substructures

Abstract

Glycans are fundamental cellular building blocks, involved in many organismal functions. Advances in glycomics are elucidating the roles of glycans, but it remains challenging to properly analyze large glycomics datasets, since the data are sparse (each sample often has only a few measured glycans) and detected glycans are non-independent (sharing many intermediate biosynthetic steps). We address these challenges with GlyCompare, a glycomic data analysis approach that leverages shared biosynthetic pathway intermediates to correct for sparsity and non-independence in glycomics. Specifically, quantities of measured glycans are propagated to intermediate glycan substructures, which enables direct comparison of different glycoprofiles and increases statistical power. Using GlyCompare, we studied diverse N-glycan profiles from glycoengineered erythropoietin. We obtained biologically meaningful clustering of mutant cell glycoprofiles and identified knockout-specific effects of fucosyltransferase mutants on tetra-antennary structures. We further analyzed human milk oligosaccharide profiles and identified novel impacts that the mother's secretor-status on fucosylation and sialylation. Our substructure-oriented approach will enable researchers to take full advantage of the growing power and size of glycomics data.

41 ## Introduction

42 Glycosylation is a highly abundant and complex post-translational modification, decorating
43 between one-fifth and one-half of eukaryotic proteins[1,2]. These diverse carbohydrates account for
44 12-25% of dry cell mass and have important functional and pathological roles[3,4]. Despite their
45 importance, glycans have complex structures that are difficult to study. The complex structures
46 of glycans arise from a non-template driven synthesis through a biosynthetic network involving
47 dozens of enzymes. A simple change of a single intermediate glycan or glycosyltransferase will
48 have cascading impacts on the final glycans obtained[5,6]. Unfortunately, current data analysis
49 approaches for glycoprofiling and glycomic data lack the necessary systems perspective to easily
50 decode the interdependency of glycans. It is important to understand the network behind the
51 glycoprofiles so that we can better understand the behavior of the process.

52 New tools aiding in the acquisition and aggregation of glycoprofiles are emerging, making
53 large-scale comparisons of glycoprofiles possible. Advances in mass spectrometry now enable
54 the rapid generation of many glycoprofiles with detailed glycan composition[7–10], exposing the
55 complex and heterogeneous glycosylation patterns on lipids and proteins[11,12]. Large glycoprofile
56 datasets and supporting databases are also emerging, including GlyTouCan[13], UnicarbDB[14],
57 GlyGen and UniCarbKB[15].

58 These new technologies and databases provide opportunities to examine global trends in
59 glycan function and their association with disease. However, the rapid and accurate comparison
60 of glycoprofiles can be challenging with the size, sparsity and heterogeneity of such datasets.
61 Indeed, in any one glycoprofile, only a few glycans may be detected among the thousands of
62 possible glycans[16]. Thus, if there is a major perturbation to glycosylation in a dataset, few
63 glycans, if any, may overlap between samples. However, these non-overlapping glycans may

64 only differ in their synthesis by as few as one enzymatic step. Thus, it can be difficult to know
65 which glycans to compare. Furthermore, since glycans often share substantial portions of their
66 biosynthetic pathways with each other, statistical methods that assume independence (e.g., t-
67 tests, ANOVA, etc) are inappropriate for glycomics. Here we address these challenges by
68 proposing glycan substructures, or intermediates, as the appropriate functional units for
69 meaningful glycoprofile comparisons, since each substructure can capture one step in the
70 complex process of glycan synthesis. Thus, using substructures for comparison, we account for
71 the shared dependencies across glycans.

72 Previous work has investigated the similarity across glycans using glycan motifs, such as,
73 glycan fingerprinting to describe glycan diversity in databases[17], align glycan structures[18],
74 identify glycan epitopes in glycoprofiles[19], deconvolve LC-MS data to clarify glycan
75 abundance[20], or compare glycans in glycoprofiles leveraging simple structures[21]. These tools use
76 information on glycan composition or epitopes; however, further accounting for shared
77 biosynthetic steps across glycans could provide complete biosynthetic context to all glycan
78 epitopes. That context includes connecting all glycans to the enzymes involved in their synthesis,
79 the order of the enzyme reactions, and information on competition for glycan substrates. Thus, a
80 generalized substructure approach could facilitate the study of large numbers of glycoprofiles by
81 connecting them to the shared mechanisms involved in making each glycan.

82 Here we present GlyCompare, a method enabling the rapid and scalable analysis and
83 comparison of any number of glycoprofiles, while accounting for the biosynthetic similarities of
84 each glycan. This approach addresses current challenges in sparsity and hidden interdependence
85 across glycomic samples, and will facilitate the discovery of mechanisms underlying the changes
86 among glycoprofiles. We demonstrate the functionality and performance of this approach with

87 both protein-conjugated and unconjugated glycomic analysis, using recombinant erythropoietin
88 (EPO) N-glycosylation and human milk oligosaccharides (HMOs). Specifically, we analyzed
89 sixteen MALDI-TOF glycoprofiles of EPO, where each EPO glycoprofile was produced in a
90 different glycoengineered CHO cell line[9,11]. We also analyzed forty-eight HPLC glycoprofiles of
91 HMO from six mothers[22]. By analyzing these glycoprofiles with GlyCompare, we quantify the
92 abundance of important substructures, cluster the glycoprofiles of mutant cell lines, connect
93 genotypes to unexpected changes in glycoprofiles, and associate a phenotype of interest with
94 substructure abundance and flux. We further demonstrate that such analyses gain statistical
95 power since GlyCompare elucidates and uses shared intermediates. The analysis of the EPO and
96 HMO datasets demonstrate that our novel framework presents a convenient and automated
97 approach to elucidate novel insights into complex patterns in glycobiology.

98 **Results**

99 **Glycomic data may fail to recover biologically meaningful clusters**

100 Due to the sparsity and non-independence of glycoprofile, clustering and comparing different
101 glycoprofiles can be challenging[23]. We tested this by clustering glycoprofiles from a panel of
102 different Erythropoietin (EPO) glycoforms, each produced in different glycoengineered CHO
103 cell lines. In the clustering, many neighboring samples were not coming from the most
104 genetically similar mutants, and thus did not recapitulate the severity of glycosylation disruption
105 (**Fig. 1a and Supplementary Fig. 1**). These challenges prompted us to develop GlyCompare, a
106 substructure-based approach to glycan analysis. Using GlyCompare, we decomposed the
107 glycoprofiles of glycoengineered EPO into glyco-motif abundance profiles and easily recovered
108 the expected severity of glycoengineered effects (**Fig. 1b**). The glyco-motif abundances mitigate

major statistical challenges of working with glycoprofiles. In the next section, we describe how we decompose glycoprofiles into glyco-motif abundance profiles.

GlyCompare decomposes glycoprofiles to facilitate glycoprofile comparison

Glycoprofiles can be decomposed into abundances of glycan intermediate substructures. The resulting substructure profile has richer information than whole glycan profiles and enables more precise comparison across conditions. Since glycan biosynthesis involves long, redundant pathways, the pathways can be collapsed to obtain a subset of substructures while preserving the information of all glycans in the dataset. We call this minimal set of substructures "glyco-motifs." The GlyCompare workflow consists of several steps wherein glycoprofiles are annotated and decomposed, glyco-motifs are prioritized, and each glyco-motif is quantified for subsequent comparisons. The specific workflow is described as follows.

First, to characterize each glycoprofile with substructures, all substructures in the glycoprofiles are identified and occurrence per glycan is quantified (**Fig. 1c-d**). Thus, a complete set of glycan substructures is obtained for all glycans in all glycoprofiles being analyzed. For each glycoprofile, the abundance of each substructure is calculated by summing the abundance of all glycans containing the substructure. This results in a substructure profile, which stores abundances for all glycan substructures (**Fig. 1e**) in given glycoprofile. The summation over similar structures asserts that similar structures follow the same synthetic paths, which is appropriate for glycosylation wherein synthesis is hierarchical and acyclic (**Supplementary Fig. 2,3**). Therefore, a substructure abundance is not simply a sum over similar structures, it is a meaningful sum over biosynthetic pathways.

Second, to identify the most informative substructures (i.e., glyco-motifs), substructures are

132 prioritized using the substructure network. The substructure network is built by connecting all
133 substructures with biosynthetic steps (**Fig. 1f**). Starting from the monosaccharides, each level of
134 the network represents another biosynthetic step, with one more monosaccharide than the
135 previous level. The edges in the network represent enzymatic additions of each monosaccharide.
136 These edges are weighted by the correlation between the abundances of the substrate and product
137 substructures across all samples. Redundant substructures can be easily identified since their
138 parent-child substructure abundances will be perfectly correlated. Substructure network
139 reduction proceeds by collapsing links with a perfect correlation between substrate and product
140 substructures, and only retaining the product substructure (see methods section for further
141 details). We demonstrate this network reduction in **Fig. 1f**. We identify redundant substructures
142 when the abundance of parent substructures and descendant substructure are perfectly correlated
143 across all glycoprofiles (connected with solid arrow). We remove the parent substructure
144 (substrate) while keeping the child substructure (product). The remaining substructures are
145 termed glyco-motifs; they completely describe the variance at the substructure level. The
146 abundances of all glyco-motifs are then represented as a glyco-motif profile, the minimal subset
147 of meaningful substructure abundances represent glycoprofiles (**Fig. 1f**).
148 For larger datasets, summarizing the glyco-motifs becomes necessary. Glyco-motif vectors,
149 like glycoprofiles, can be clustered (**Fig. 1g and Supplementary Fig. 4**). We defined a
150 representative substructure as the common structure in a glyco-motif cluster (**Fig. 1h**). The
151 representative substructure describes the glycan features that vary the most across samples. To
152 extract the common structural features in each cluster, we calculated the average weight of each
153 monosaccharide. Monosaccharides with a weight larger than 51% are preserved, which

154 illustrates the predominant structure in the cluster. This allows one to quickly evaluate the
155 distinguishing glycan features that vary across samples in any given dataset.
156 The workflow we described here successfully connects all glycoprofiles in a data set through
157 their shared intermediate substructures, thus allowing robust analysis of the differences across
158 glycomics samples and the evaluation of the associated genetic bases.
159
160 **GlyCompare accurately clusters glycoengineered EPO samples**
161 The poor clustering of the engineered EPO glycosylation data[9] included clustering of
162 glycoprofiles with low phenotypic similarity (**Fig. 1a and Supplementary Fig. 1,5**). This
163 inconsistency and poor clustering stems from the inherent sparseness of glycoprofiles, i.e., each
164 glycoprofile only has a few glycans. Thus, the matrix of all samples is very sparse, unfit for
165 standard clustering approaches and hard to interpret. Particularly problematic is that pairs of
166 glycans differing in a single monosaccharide are treated as two completely different glycans
167 under standard clustering approaches. Thus, we found that clustering is affected more by the
168 presence or absence of a glycan, rather than structural similarity.
169 GlyCompare addresses these problems by elucidating hidden similarities between glycans
170 after decomposing glycoprofiles to their composite substructures. The 52 glycans were
171 decomposed into their constituent glycan substructures, resulting in a substructure vector with
172 613 glycan substructures and a further simplified 120 glyco-motif vector (**Supplementary Fig.**
173 **6**). The glyco-motif clustering clearly distinguished the samples based on the structural patterns
174 and separated profiles into groups more consistently associated with the extent of changes in the
175 profile than the raw glycan-based clusters (**Fig. 1b and Supplementary Fig. 5**).

176 The sixteen glycoprofiles clustered into three groups with a few severely modified outliers
177 (**Fig. 1b**), and the 120 glyco-motifs clustered into twenty-four groups, each summarized by
178 representative substructures Rep1 - Rep24 (**Fig. 2a and Supplementary Fig. 4**). The clusters of
179 glycoprofiles are consistent with the genetic similarities among the host cells. Specifically, the
180 major substructure patterns cluster individual samples into four categories: 'wild-type (WT)-
181 like', 'mild', 'medium' and 'severe'. The WT-like category contains one group, WT and
182 B4galt1/2/3/4/ knockouts, which contains most of the substructures seen in WT cells. The mild
183 group includes the Mgat4b/4a, Mgat4b, and Mgat5 knockouts, where each lose the tetra-
184 antennary structure, and an St3gal4/6 knockout, which loses the terminal sialylation. The
185 medium category is a group that contains knockouts of St3gal4/6 and Mgat4a/4b/5, knockouts of
186 Mgat4a/4b/5 and B3gnt2, knockouts of Mgat4a/4a/5 with a knock-in of human ST6GAL1, and
187 knockouts of Mgat4a/4b/5 and St3gal4/6. The medium disruption category lost the tri-antennary
188 structure. The 'severe' category includes three individual glycoprofiles with knockouts for Fut8,
189 Mgat2, and Mgat1, each of which generate many glycans not detected in the WT-like, mild or
190 medium categories. While some glyco-motif clusters can be seen in the glycoprofile clusters,
191 there are important differences, and the glyco-motif clusters provide more information and
192 improved cluster stability (**Supplementary Fig. 4,7**). These results demonstrate the performance
193 improvement of glyco-motif abundance over glycan abundance in assessing the structural
194 similarity between different glycoprofiles.
195
196 **GlyCompare summarizes structural changes across glycoprofiles**
197 GlyCompare helps to more robustly group samples by accounting for the biosynthetic and
198 structural similarities of glycans. Further analysis of the representative structures provides

199 detailed insights into which structural features vary the most across samples. To accomplish this,
200 we rescaled the representative structure abundances and identified significant changes in
201 representative substructure abundances between mutant cells and WT (**Fig. 2a,b**). This highlights
202 the specific structural features of glycans that are impacted when glycoengineering recombinant
203 EPO.

204 As expected, in the Mgat1 knockout glycoprofile, only high mannose N-glycans are seen.
205 Also, in the Mgat2 knockout, the glycan substructure of bi-antennary on one mannose linkage
206 significantly increases, and the unique structure of bi-antennary LacNac elongated in the N-
207 glycans emerges in the St3gal4/6 and Mgat4a/4b/5 knockouts. Along with expected changes in
208 α-1,6 fucosylation in the Fut8 knockout glycoprofile, we also observed an increase in the tetra-
209 antennary poly-LacNac elongated N-glycan without fucose, which has not been previously
210 reported (One-sided one-sample wilcoxon test, Rep19: p=2.7×10^{-4}, Rep21: p=2.0×10^{-4})
211 (**Fig. 2c**). In the St3gal4/6 knockout (**Fig. 2c**), we observed the relative abundance of structures
212 with sialylation significantly decreased, while the tetra-antennary and triantennary poly-LacNAc
213 elongated N-glycan substructure without sialylation significantly increased (Rep13: p=
214 1.3×10^{-3}, Rep20: p=2.3×10^{-4}). Finally, the Mgat4b, Mgat4a/4b and Mgat5 knockouts (**Fig.
215 2d**) lose all core tetra-antennary substructures (Rep16: unscaled abundance=0). While
216 triantennary substructures with GlcNac elongation increased significantly for Mgat4b (Rep13:
217 p=2.6×10^{-3}, Rep14: p=2.5×10^{-4}), the poly-LacNac elongation structure disappeared.
218 Interestingly, while both the Mgat4b and Mgat5 knockouts do not have the tri-antennary poly-
219 LacNac elongated N-glycan, the Mgat4a/4b mutant keeps a highly abundant poly-LacNac branch
220 (Rep15: p= 2.4×10^{-4}). Thus, through the use of GlyCompare, we identified the specific glycan

221 features that are impacted not only in individual glycoengineered cell lines, but also features
222 shared by groups of related cell lines.
223
224 **GlyCompare reveals phenotype-associated substructures and trends invisible at the whole**
225 **glycan level**
226 Many secreted and measured glycans are also precursors, or substructures, of larger glycans (**Fig.**
227 **3a**). Thus, the secreted and observed abundance of one glycan may not equal to the total amount
228 synthesized. GlyCompare can quantify the total abundance of a glycan by combining the glycan
229 abundance with the abundance of its products. To demonstrate this capability of GlyCompare,
230 we analyzed HMO abundance, and examined the impact of secretor status and days postpartum
231 on HMO abundance. We obtained forty-seven HMO glycoprofiles from 6 mothers (1, 2, 3, 4, 7,
232 14, 28 and 42 days postpartum (DPP)), 4 "secretor" mothers with functioning FUT2 (α-1,2
233 fucosyltransferase), and 2 "non-secretor" mothers with non-functional FUT2. With GlyCompare
234 addressing the non-independence of HMOs, we could use powerful statistical methods to study
235 trends in HMO synthesis. Specifically, we used regression models predicting secretor status and
236 DPP from substructure abundance.
237 We first checked both the glycan-level and substructure-level clustering of the glycoprofile.
238 Samples with same secretor status and days postpartum (DPP) were successfully grouped
239 (**Supplementary Fig. 8**). Further examination of the glyco-motif abundance (i.e., the total
240 amount of substructure synthesized) revealed phenotype-related trends invisible at the level of
241 the whole glycan profile. For example, the LSTb substructure (X62) increased in secretor
242 mothers (Wald $p = 2 \times 10^{-16}$) and decreased in non-secretor mothers over time (Wald $p <$
243 2×10^{-16}; **Fig. 3b**). Yet, the same trend was weak or inconsistent for all glycans containing the

244 X62 substructure: LSTb, DSLNT and DSLNH (**Fig. 3b-e)**. LSTb weakly shows a similar trend
245 to X62. LSTb decreases over time in non-secretors (Wald p = 6.53×10^{-4}) but the time-
246 dependent increase in secretors is barely significant (Wald p = 0.046) and the effect size is small
247 (marginal R^2 = 0.088). Unlike X62, DSLNT shows no significant increase over time (Coef=-
248 0.39, Wald p = 0.17) in secretor mothers. Finally, unlike the decrease over time seen in non-
249 secretors in X62, DSLNH shows a significant increase over time in non-secretors (Wald p =
250 2.91×10^{-8}). The secretor-specific trends in total LSTb are only clearly visible by examining the
251 X62 substructure abundance (**Fig. 3c**). Thus, while secretor status is expected to impact HMO
252 fucosylation, GlyCompare reveals associations with non-fucosylated substructures. Viewing
253 substructure abundance as total substructure synthesized provides a new fundamental measure to
254 the study of glycoprofiles, it also creates an opportunity to explore trends in synthesis.
255

256 **GlyCompare identifies flux in HMO biosynthesis**

257 We next applied GlyCompare to explore changes in HMO synthesis over time. For this, we
258 estimate the flux for each biosynthetic reaction by quantifying the abundance ratio of products
259 and substrates from parent-child pairs of glycan substructures. Thus, we could study changes in
260 HMO synthesis through the systematic estimation of reaction flux across various conditions.
261 We found several reactions strongly associated with secretor status. As expected, the estimated
262 reaction flux from the LNT substructure (X40) to the LNFPI substructure (X65), was strongly
263 associated with secretor status (Wilcox p =1.3×10^{-12}). In secretors, 36.2% (s.d. 12.7%) of X40
264 was converted to X65, compared to non-secretors, wherein only 5% (s.d. 1.3%) of X40 was
265 converted.

266 Although secretor status is defined by the fucosyltransferase-2 genotype, not all secretor-
267 associated reactions were fucosylation reactions. We further explored the secretor-X62
268 association using the product-substrate ratio to estimate flux. Specifically, we examined the
269 upstream reaction (**Fig. 3f)** of LNT (X40) to LSTb (X62) and the downstream reaction (**Fig. 3g)**
270 of LSTb (X62) to DSLNT (X106). We measured the upstream reaction of LNT converting to
271 LSTb, using the X62/X40 ratio over time, however, no significant change was observed with
272 respect to secretor status (Wald p=0.55). In the conversion of LSTb to DSLNT, we found a
273 secretor-specific reaction increase in flux. Specifically, the X106/X62 ratio was significantly
274 higher (Wald p=0.018) in secretor mothers (**Fig. 4g; Supplementary Table 3c)** In the average
275 non-secretor mother, 52.3% (s.d. 15.1%) of LSTb is converted to DSLNT. Meanwhile in
276 secretors, the average conversion rate is 81.8% (s.d. 7.2%). The LSTb to DSLNT conversion rate
277 appears higher in secretors while conversion from the LSTb precursor, LNT, appears unchanged;
278 any changes in sialylation is intriguing, considering secretor status is associated with genetic
279 variation of a fucosyltransferase. Examining the product-substrate ratio has revealed a
280 phenotype-specific reaction propensity thus providing insight to the condition-specific synthesis.
281

282 **GlyCompare increases statistical power of glycomics data**

283 GlyCompare successfully provides new insights by accounting for shared biosynthetic routes of
284 measured oligosaccharides. Since it includes information on the similarities between different
285 glycans, we wondered how our approach impacts statistical power in glycan analysis. Thus, to
286 quantify the benefit of glyco-motif analysis, we constructed a large number of regression models
287 associating either glyco-motif abundance or glycan abundance, with a DPP and secretor status
288 (see **Methods**). We found that regressions trained with glyco-motif abundance are more robust

289 than those trained on whole glycan HMO abundance, as indicated by the increased coefficient
290 magnitude (Wilcoxon p = 0.0047, **Fig. 4a**), and decreased standard error (Wilcoxon p = 0.033,
291 **Fig. 4b**). An increase in the stability of a statistic can result in an increased effect size. Consistent
292 with the increased coefficient magnitude and decreased standard error, the effect size also
293 increased, as measured by the marginal R^2 (mR^2) of glyco-motif-trained regressions (Wilcoxon
294 p=0.04, **Fig. 4c**). These effects were confirmed with a bootstrapping t-test; bootstrapping p-
295 values were less than or equal to Wilcoxon p-values within 0.001. Increases in statistic
296 magnitude, statistic stability, and effect size are all expected to increase the power of an analysis.
297 Using the median, 1st quartile, and 3rd quartile of observed mR^2, we estimated the expected
298 power of glyco-motif-trained and glycan-trained regressions at various sample sizes. The
299 expected power of a glyco-motif-trained regression reaches 0.8 at 36 samples and 0.9 with 57
300 samples while a glycan-trained regression requires more than double the sample size to reach a
301 comparable power (**Fig. 4d**). Thus, using GlyCompare for glyco-motif-level analysis can
302 substantially increase the robustness and statistical power in glycomics data analysis since it
303 allows for the comparison of different glycans who share biosynthetic steps.

304 Discussion

305 Glycosylation has generally been studied from the whole-glycan perspective using mass
306 spectrometry and other analytical methods. From this perspective, two glycans that differ by only
307 one monosaccharide are distinct and are not directly comparable. Thus, the comparative study of
308 glycoprofiles has been limited to changes between glycans shared by multiple glycoprofiles or
309 small manually curated glycan substructures[17]. GlyCompare sheds light on the hidden
310 biosynthetic interdependencies between glycans by integrating the biosynthetic pathways into the

311 comparison. Glycoprofiles are converted to glyco-motif profiles, wherein each substructure
312 abundance represents the cumulative abundance of all glycans containing that substructure. This
313 enumeration and quantification of substructures can be easily scaled up to include many
314 glycoprofiles in large datasets. Additionally, since no prior information is required beyond
315 glycan identities and quantities, the method can even facilitate analysis of glycans with limited
316 characterization. Thus, it brings several advantages and new perspectives to enable the
317 systematic study of glycomics data.

318 First, the GlyCompare platform computes a glyco-motif profile (i.e., the abundances of the
319 minimal set of glycan substructures) that maintains the information of the original glycoprofiles,
320 while exposing the shared intermediates of measured glycans. These sample-specific glyco-motif
321 profiles more accurately quantify similarities across glycoprofiles. This is made possible since
322 glycans that share substructures also share many biosynthetic steps. If the glycan biosynthetic
323 network is perturbed, all glycans synthesized will be impacted and the nearest substructures will
324 directly highlight where the change occurred. For example, in EPO glycoprofiles studied here,
325 the tetra-antennary structure is depleted in the Mgat4a/4b/5 knockout group and the downstream
326 sialylated substructure depleted when St3gal4/6 were knocked out. Such structural patterns
327 emerge in GlyCompare since the tool leverages shared intermediate substructures for clustering,
328 thus identifying common features in glycans measured across diverse samples.

329 Second, new trends in glycan biosynthetic flux become visible at the substructure level. For
330 example, in the HMO data set, multiple HMOs are made through a series of steps from LNT to
331 DSLNH (**Fig. 4a**). Only when the substructure abundances and product-substrate ratios are
332 computed are we able to observe the secretor-dependent differences in the abundance of the
333 LSTb substructure, X62. This is particularly interesting since secretor status is defined by

334 changes in α-1,2 fucosylation, but we see here additional secretor-dependent changes to
335 sialylated structures with no fucose. These are the systemic effects invisible without a systems-
336 level perspective due to the interconnected nature of glycan synthesis; this disparity underlines
337 the power of this method.

338 Third, the sparse nature of glycomic datasets and the synthetic connections between glycans
339 make glycomic data unfit for many common statistical analyses. However, the translation of
340 glycoprofiles into substructure abundance provides a framework for more statistically powerful
341 and robust analysis of glycomic datasets. Single sample perturbations, such as the knockouts in
342 the glycoengineered EPO, can be compared to wild-type; all substructure data can be normalized
343 and then rigorously distinguished from the control using a one sample Wilcoxon-test.
344 Furthermore, conditions or phenotypes with many glycoprofiles, such as the secretor status in the
345 HMO dataset, can be compared using a variety of statistical methods to evaluate the association
346 between the phenotypes and glycosylation. For example, in HMO data, we revealed that the α-
347 1,2 fucose substructure is enriched in secretor status, consistent with the previous studies[24–26].
348 Because the substructure approach includes comparisons of glycans that are not shared across the
349 different samples, but that share intermediates, GlyCompare decreased sparsity and increased
350 statistical power. Thus, one can obtain richer glycan comparisons of representative substructures,
351 total synthesized abundance, and flux.

352 Finally, in combination with the substructure network, we can systematically study glycan
353 synthesis. The product-substrate ratio provides an estimation of flux through the glycan
354 biosynthetic pathways. Using the HMO dataset, we demonstrate the power of this perspective by
355 showing that more LSTb is converted to DSLNT in the secretor mother. The perspectives made
356 available through GlyCompare are not limited to Wilcoxon-tests and regression models. Because

357 the substructure-level perspective minimizes biosynthetic dependency between glycans, glyco-
358 motif abundances can be used with nearly any statistical model or comparison demanded by a
359 dataset. We have reduced the sparse and non-independent nature of glycoprofiles, thereby
360 making countless comparisons and new analyses possible.
361

362 **Conclusions**

363 In conclusion, GlyCompare provides a novel paradigm for describing complex glycoprofiles,
364 thus enabling a wide range of analyses and facilitating the acquisition of detailed insights into the
365 molecular mechanisms controlling all types of glycosylation.
366

367 **Acknowledgements**

368 Many thanks to Joshua Klein for providing guidance on using glypy
369 (https://github.com/mobiusklein/glypy). Thanks to Philip Gordts for insightful comments. This
370 work was conducted with support from the Novo Nordisk Foundation provided to the Center for
371 Biosustainability at the Technical University of Denmark (NNF10CC1016517: A.W.T.C.),
372 NIGMS (R35 GM119850: B.B., B.K.P., N.E.L.) , NICHD (R21 HD080682: L.B.) and USDA
373 (USDA/ARS 6250-6001; M.W.H). This work is a publication of the U.S. Department of
374 Agriculture/Agricultural Research Service, Children's Nutrition Research Center, Department of
375 Pediatrics, Baylor College of Medicine, Houston, Texas. The contents of this publication do not
376 necessarily reflect the views or policies of the U.S. Department of Agriculture, nor does mention
377 of trade names, commercial products, or organizations imply endorsement from the U.S.
378 government.
379

Author contributions

B.B, B.P.K. designed the work. B.B., B.P.K., A.W.T.C., A.K.Y., and N.E.L. performed data analysis. M.A.M., M.W.H., and L.B. provided HMO data. The manuscript was written by B.B., B.P.K., A.W.T.C., L.B., and N.E.L.

Competing interests

The authors declare no competing financial interests.

388 **References**

389 1. Khoury, G. A., Baliban, R. C. & Floudas, C. A. Proteome-wide post-translational modification
390 statistics: frequency analysis and curation of the swiss-prot database. *Sci. Rep.* **1**, (2011).
391 2. Apweiler, R., Hermjakob, H. & Sharon, N. On the frequency of protein glycosylation, as deduced
392 from analysis of the SWISS-PROT database. *Biochim. Biophys. Acta* **1473**, 4–8 (1999).
393 3. RodrÍguez, E., Schetters, S. T. T. & van Kooyk, Y. The tumour glyco-code as a novel immune
394 checkpoint for immunotherapy. *Nat. Rev. Immunol.* **18**, 204–211 (2018).
395 4. Gutierrez, J. M. *et al.* Genome-scale reconstructions of the mammalian secretory pathway predict
396 metabolic costs and limitations of protein secretion. *bioRxiv* 351387 (2018). doi:10.1101/351387
397 5. Gabius, H.-J., André, S., Kaltner, H. & Siebert, H.-C. The sugar code: functional lectinomics.
398 *Biochimica et Biophysica Acta (BBA) - General Subjects* **1572**, 165–177 (2002).
399 6. Spahn, P. N. & Lewis, N. E. Systems glycobiology for glycoengineering. *Curr. Opin. Biotechnol.*
400 **30**, 218–224 (2014).
401 7. Holst, S. *et al.* N-glycosylation Profiling of Colorectal Cancer Cell Lines Reveals Association of
402 Fucosylation with Differentiation and Caudal Type Homebox 1 (CDX1)/Villin mRNA Expression.
403 *Mol. Cell. Proteomics* **15**, 124–140 (2016).
404 8. Reiding, K. R., Blank, D., Kuijper, D. M., Deelder, A. M. & Wuhrer, M. High-throughput profiling
405 of protein N-glycosylation by MALDI-TOF-MS employing linkage-specific sialic acid esterification.
406 *Anal. Chem.* **86**, 5784–5793 (2014).
407 9. Yang, Z. *et al.* Engineered CHO cells for production of diverse, homogeneous glycoproteins. *Nat.*
408 *Biotechnol.* **33**, 842–844 (2015).
409 10. Anugraham, M. *et al.* Specific glycosylation of membrane proteins in epithelial ovarian cancer cell
410 lines: glycan structures reflect gene expression and DNA methylation status. *Mol. Cell. Proteomics*
411 **13**, 2213–2232 (2014).
412 11. Čaval, T., Tian, W., Yang, Z., Clausen, H. & Heck, A. J. R. Direct quality control of

413 glycoengineered erythropoietin variants. *Nat. Commun.* **9**, 3342 (2018).
414 12. Riley, N. M., Hebert, A. S., Westphall, M. S. & Coon, J. J. Capturing site-specific heterogeneity
415 with large-scale N-glycoproteome analysis. *Nat. Commun.* **10**, 1311 (2019).
416 13. Aoki-Kinoshita, K. *et al.* GlyTouCan 1.0--The international glycan structure repository. *Nucleic*
417 *Acids Res.* **44**, D1237–42 (2016).
418 14. Campbell, M. P. *et al.* Validation of the curation pipeline of UniCarb-DB: building a global glycan
419 reference MS/MS repository. *Biochim. Biophys. Acta* **1844**, 108–116 (2014).
420 15. Campbell, M. P. *et al.* UniCarbKB: building a knowledge platform for glycoproteomics. *Nucleic*
421 *Acids Res.* **42**, D215–21 (2014).
422 16. Cummings, R. D. The repertoire of glycan determinants in the human glycome. *Mol. Biosyst.* **5**,
423 1087–1104 (2009).
424 17. Rademacher, C. & Paulson, J. C. Glycan fingerprints: calculating diversity in glycan libraries. *ACS*
425 *Chem. Biol.* **7**, 829–834 (2012).
426 18. Hosoda, M. *et al.* MCAW-DB: A glycan profile database capturing the ambiguity of glycan
427 recognition patterns. *Carbohydr. Res.* **464**, 44–56 (2018).
428 19. Alocci, D. *et al.* Understanding the glycome: an interactive view of glycosylation from
429 glycocompositions to glycoepitopes. *Glycobiology* **28**, 349–362 (2018).
430 20. Klein, J., Carvalho, L. & Zaia, J. Application of network smoothing to glycan LC-MS profiling.
431 *Bioinformatics* **34**, 3511–3518 (2018).
432 21. Sharapov, S. *et al.* Defining the genetic control of human blood plasma N-glycome using genome-
433 wide association study. *bioRxiv* 365486 (2018). doi:10.1101/365486
434 22. Mohammad, M. A., Hadsell, D. L. & Haymond, M. W. Gene regulation of UDP-galactose synthesis
435 and transport: potential rate-limiting processes in initiation of milk production in humans. *Am. J.*
436 *Physiol. Endocrinol. Metab.* **303**, E365–76 (2012).
437 23. Ashwood, C., Pratt, B., MacLean, B. X., Gundry, R. L. & Packer, N. H. Standardization of PGC-LC-
438 MS-based glycomics for sample specific glycotyping. *Analyst* **144**, 3601–3612 (2019).

439 24. Koda, Y., Soejima, M., Liu, Y. & Kimura, H. Molecular basis for secretor type alpha(1,2)-
440 fucosyltransferase gene deficiency in a Japanese population: a fusion gene generated by unequal
441 crossover responsible for the enzyme deficiency. *Am. J. Hum. Genet.* **59**, 343–350 (1996).
442 25. Kudo, T. *et al.* Molecular genetic analysis of the human Lewis histo-blood group system. II. Secretor
443 gene inactivation by a novel single missense mutation A385T in Japanese nonsecretor individuals. *J.*
444 *Biol. Chem.* **271**, 9830–9837 (1996).
445 26. Viverge, D., Grimmonprez, L., Cassanas, G., Bardet, L. & Solere, M. Discriminant carbohydrate
446 components of human milk according to donor secretor types. *J. Pediatr. Gastroenterol. Nutr.* **11**,
447 365–370 (1990).
448 27. Mohammad, M. A. & Haymond, M. W. Regulation of lipid synthesis genes and milk fat production
449 in human mammary epithelial cells during secretory activation. *Am. J. Physiol. Endocrinol. Metab.*
450 **305**, E700–16 (2013).
451 28. Bode, L. *et al.* Human milk oligosaccharide concentration and risk of postnatal transmission of HIV
452 through breastfeeding. *Am. J. Clin. Nutr.* **96**, 831–839 (2012).
453 29. Alderete, T. L. *et al.* Associations between human milk oligosaccharides and infant body
454 composition in the first 6 mo of life. *Am. J. Clin. Nutr.* **102**, 1381–1388 (2015).
455 30. Rosenthal, R. & Rubin, D. B. Further issues in effect size estimation for one-sample multiple-choice-
456 type data. *Psychological Bulletin* **109**, 351–352 (1991).
457 31. Yan, J. & Fine, J. Estimating equations for association structures. *Stat. Med.* **23**, 859–74; discussion
458 875–7,879–80 (2004).
459 32. Halekoh, U., Højsgaard, S., Yan, J. & Others. The R package geepack for generalized estimating
460 equations. *J. Stat. Softw.* **15**, 1–11 (2006).
461 33. Zeger, S. L. & Liang, K. Y. Longitudinal data analysis for discrete and continuous outcomes.
462 *Biometrics* **42**, 121–130 (1986).
463 34. Zheng, B. Summarizing the goodness of fit of generalized linear models for longitudinal data. *Stat.*
464 *Med.* **19**, 1265–1275 (2000).

465 # Methods

466 **Data, source code, examples, Jupyter notebooks for generating manuscript figures, and**
467 **CodeOcean capsule available at:**
468 **https://github.com/LewisLabUCSD/GlyCompare**
469

470 **N-glycosylation of EPO glycoprofile collection and analysis**

471 N-glycosylation data were previously published and described elsewhere[9]. Briefly, these data
472 were generated as follows. Different combinations of glycosyltransferase genes were knocked
473 out using zinc-finger nucleases. Both single gene and multigene mutants were generated.
474 Erythropoietin (EPO) was transfected into the library of glycoengineered cell lines. After
475 overexpression of EPO, glycans were cleaved using PNGase, and then assayed by mass
476 spectrometry. Upon retrieval of these data from the study, we picked 16 glycoprofiles that are
477 used again in their following up study [11] and further processed the data as follows. All
478 measurements were taken from distinct samples.

479 Glycan substructures were extracted from the observed glycans. Substructure abundance was
480 calculated from glycan abundance of all glycans containing the substructure. A minimal set of
481 120 glyco-motifs substructures identified by substructure network to compare the mutants.
482 Finally, representative substructures were extracted to pool abundance and summarize the
483 structural changing across mutants. Each of these operations is further specified below.
484

485 **HMO glycoprofile collection and analysis**

486 Following Institutional Review Board approval (Baylor College of Medicine, Houston, TX),
487 lactating women were given written informed consent. Women with diabetes or impaired

488 glucose tolerance, anemia, or renal or hepatic dysfunction were excluded from the study. Women
489 were 18-35 years of age, had uncomplicated singleton pregnancies with vaginal delivery at term
490 (>37 weeks) and pregnancy Body Mass Index (BMI) remained <26kg/m2. Infants were healthy
491 and exclusively breastfed. Forty-eight milk samples were collected from 6 human mothers (1, 2,
492 3, 4, 7, 14, 28, and 42 days postpartum (DPP)). More information on subject selection, exclusion,
493 study design, and breast milk collection has already been published [22,27]
494 HMO composition and abundance was measured by high-performance liquid chromatography
495 (HLPC) following fluorescent derivatization with 2-aminobenzamide (2AB, CID: 6942) as
496 previously described [28,29]. Raffinose (CHEBI:16634, CID:439242), a non-HMO oligosaccharide,
497 was added to each milk sample as an internal standard at the very beginning of sample
498 preparation to allow for absolute quantification. Of the 300-500 predicted HMO, the 16 most
499 abundant HMO were detected based on retention time comparison with commercial standard
500 oligosaccharides and mass spectrometry analysis including 2-fucosyllactose (2'FL), 3-
501 fucosyllactose (3'FL), 3-sialyllactose (3'SL), lacto-N-tetrose (LNT), lacto-N-neotetraose (LNnT),
502 lacto-N-fucopentaose (LNFP1, LNFP2 and LNFP3), sialyl-LNT (LSTb and LSTc), difucosyl-
503 LNT (DFLNT), disialyllacto-N-tetraose (DSLNT), fucosyl-lacto-N-hexaose (FLNH), difucosyl-
504 lacto-N-hexaose (DFLNH), fucosyl-disialyl-lacto-N-hexaose (FDSLNH) and disialyl-lacto-N-
505 hexaose (DSLNH). Because these are the most abundant HMOs, these glycoprofiles represent
506 the least sparse subset of the entire HMO glycoprofile which is extremely sparse. GlyTouCan
507 IDs for each HMO are listed in **Supplementary Table 2**. Technicians were blinded to metadata
508 associated with each sample. In addition to absolute concentrations, the proportion of each HMO
509 per total HMO concentration (sum of all integrated HMO) was calculated and expressed as

510 relative abundance (% of total, $w_i/\Sigma w_*$). The presence of 2-FL defines secretor status. All
511 measurements were taken from distinct samples.
512 HMO abundances profiles were treated similarly to the N-glycans. We identified and
513 quantified 26 glyco-motifs from 121 substructures. We compared glyco-motif abundance and
514 their abundance ratios directly to secretor status along the log of days postpartum.
515

516 **Glycoprofile preprocess procedures**

517 Three procedures were used for preprocessing the studied glycoprofiles (**Fig. 1c**). First,
518 glycoprofiles are parsed into glycans with abundance. In each glycoprofile, the glycans are
519 manually drawn and exported with GlycoCT format using the GlyTouCan Graphic Input tool[13].
520 GlycoCT formatted glycans are loaded into Python (version 3+) and initialized as glypy.glycan
521 objects using the *glypy* (version 0.12.1). Assuming we have a glycoprofile ***i***, the corresponding
522 abundance of each glycan ***j*** in glycoprofile ***i*** is represented by g_{ij}. For example, the relative m/z
523 peak in the mass spectrum or the abundance value in an HPLC trace, is calculated relative to the
524 total abundance of glycans in this glycoprofile $g_{ij}/\Sigma g_{i*}$. Glycans with ambiguous topologies are
525 handled by assuming they belong to every possible structure with equal probability, thereby
526 creating all possible ***n*** structures but with $g_{ij}/n\Sigma g_{i*}$ abundance of each. Second, glycans are
527 annotated with glycan substructure information, and this information is transformed into the
528 substructure vector. Substructures within a glycan are exhaustively extracted by breaking down
529 each linkage or a combination of linkages of the studied glycan. Note that this method cannot
530 currently deal with glycans with ring topology. All substructures extracted are merged into a
531 substructure set ***S***. Substructures are sorted by the number of monosaccharides and duplicates are
532 removed. Then, each glycan is matched to the substructure set ***S*** producing a binary glycan

533 substructure presence (1) or absence (0) vector, x_{ij}. Lastly, a substructure (abundance) vector is
534 calculated as $p_i = \Sigma x_{ij} g_{ij} / \Sigma g_{i*}$ representing the abundance of the substructures $\boldsymbol{s}$ in this
535 glycoprofile, where $p_i = (s_{1i}, \ldots, s_{ni})$. Third, a substructure network is built based on the
536 substructure vectors. The substructure network is a directed acyclic graph wherein each node
537 denotes a glycan substructure. Given the substructure set S, the root node starts from the
538 monosaccharides or a defined root core structure, and a child node is a substructure that has only
539 one monosaccharide added to its parent node. We note that one child node might have multiple
540 parent nodes and vice versa. The child node depends on its parent node(s) since it cannot exist
541 alone without any parent node.
542
543 **Generating the glyco-motif vector bases on the substructure abundance**
544 A larger subset of the substructure network is necessary to uniquely describe a more diverse set
545 of glycoprofiles while fewer substructures are needed to describe more similar glycoprofiles
546 sufficiently. Comparisons become more focused when only examining these variable
547 substructures. By checking the substructure network, the substructures that have the same
548 abundance can be merged without any information loss. In other words, after the substructure
549 network is generated, it is simplified by merging the substructure nodes. As illustrated in **Fig. 1f**,
550 the parent-child substructure pairs with perfectly correlated abundance (solid arrow), can be
551 merged. We remove the parent node while keeping the child node. Furthermore, an epitope
552 substructure can also be removed if they are 100% correlated with the bigger substructure
553 containing that epitope. Base on our rule, the merging criteria are based on how child
554 substructure node s_b depends on the parent substructure node s_a. The dependency is the Pearson
555 correlation of their abundance across all glycoprofiles, $corr(s_{a*}, s_{b*})$. If the correlation is 1, we

556 can conclude that the addition of the specific monosaccharide is not perturbed across all
557 glycoprofiles, which means they carry the same information. Thus, the parent node can be
558 pruned without information loss. All remaining nodes, namely, the glyco-motifs, are used to
559 cluster the glycoprofiles.

560 Meanwhile, we use the "monosaccharides weight" to track the nodes merging process. All
561 node weights are initialized as 1. When a node is removed, the weight is equally divided and
562 distributed to child nodes whose correlation with the removed node is 1. Since this method
563 redistributes weight from the root to leaves, the last decedent substructure node with a non-
564 unique abundance pattern gains the most weight. The weights **W** are used later for generating the
565 representative substructures.

566

567 **Procedures for glycoprofile clustering and identifying representative glycan substructures**

568 The preprocessed glycoprofiles (see details in the "glycoprofile preprocess procedures") generate
569 the substructure vectors to enable further clustering analysis. Here we used the Pearson
570 correlation and 'complete' distance to cluster the glycoprofiles. This procedure clusters the
571 glycoprofiles and substructures.

572 To identify the representative glycan substructures, a set of glycan substructures with weights
573 ***W*** are first aligned. Then, we calculate the sum of monosaccharide weights for each glycan
574 substructure. The representative substructure is thus defined as the glycan substructures with
575 their summed monosaccharide weights greater than 51% of the total weight of glycan
576 substructures. Lastly, the averaged abundances of the representative substructures are generated
577 to assess their differential expressions between different glycoprofiles.

578

579 **Test the abundance changes on representative substructures**

580 We use the representative substructures to summarize and analyze the structural and quantitative
581 changes across glycoprofiles. For the abundance of a representative substructure in a glyco-motif
582 cluster, we use the substructure monosaccharide weights to calculate the weighted average of
583 substructure abundance. Since the abundance range of representative substructures across
584 different glycoprofiles are different, we re-centralized the representative substructure abundance
585 based on WT and scaled them with standard deviation. We can find many interesting signals
586 since there are many representative substructures extremely deviating from the WT's abundance.
587 Since the abundance distributions are not normally distributed, we used a one-sided 1-sample
588 Wilcoxon test to test if the abundance of a representative substructure in a glycoprofile is
589 significantly divergent. Effect size, r, was calculated as z/sqrt(N)[30]. A Bonferroni correction
590 (n=16) was used to correct for multiple testing, so p=0.0031 is used as criteria and effect sizes
591 are all above 0.68.

592

593 **Testing the substructure-phenotype association**

594 We estimated the influence of Secretor status on HMO and glyco-motif abundance using
595 generalized estimating equation (GEE, R3.6::geepack[31,32]). GEE models account for resampling
596 bias in longitudinal measurements[33]; other regression models, like generalized linear models,
597 overestimate the sample size and power by ignoring this bias. Unlike mixed effect models, which
598 can account for resampling bias, GEE allows non-linear relations between the outcome and
599 covariates, while accounting for correlation among repeated measurements from the same
600 subject. Here we used GEE with exchangeable correlation structure (assuming the within-subject
601 correlation between any two time-points is ρ). To stabilize the variance and equalize the range,

602 we log and z-score standardized each HMO and glyco-motif measurement. We also used the log
603 of days postpartum (DPP) to linearize the relationship over time. The Wald test was used to
604 measure the significance of Secretor status contribution. For additional information and
605 diagnostic statistics for specific regressions, see **Supplementary Table 3a,b**. All regression can
606 be found in **Supplementary Fig. 9.**
607

608 **Product-substrate ratio as a proxy for flux and estimating flux-phenotype associations**

609 To further isolate glyco-motif-specific effects from biosynthetic biases, we explored methods to
610 control for the product-substrate relations. First, we isolated the relative abundance of parent-
611 child pairs of glyco-motifs in the substructure network; these are product-substrate relations like
612 LNT and LSTb. Glyco-motif abundance represents the total substructure synthesized; therefore,
613 when we examine the product-substrate ratio, we measure the total amount of the substrate
614 substructure converted to the product substructure in the sample. Thus, the product-substrate
615 ratio is a proxy for flux. Using logistic GEE regression modeling, similar to the approach used
616 for testing substructure-phenotype associations, we can measure the influence of estimated flux
617 between two glycans on secretor status; here we predicted secretor status from estimated flux
618 log(DPP). For additional information and diagnostic statistics, see **Supplementary Table 3c.**
619

620 **Glyco-motif Abundance Robustness and Power Analysis**

621 GEE models, similar to those used in **Supplementary Fig. 9**, were trained using either glyco-
622 motif or whole HMO relative abundance. To stabilize the variance, equalize the range and make
623 the regressions comparable, we used a square root and z-score normalization on each HMO and
624 glyco-motif measurement. Glyco-motif or glycan relative abundance was predicted from either

625 DPP alone, Secretor status alone, DPP + Secretor status, or DPP + Secretor status +
626 DPP:Secretor. To avoid biasing the analysis with misfit or uninformative models, models with
627 small coefficients (|coef|<0.5) or extremely non-normal abundance distributions (Shapiro-Wilks
628 $p < 0.001$) were removed. Model robustness measures including, coefficient magnitude ($n_{glycan-}$
629 $_{stats}$=39, $n_{motif-stats}$=86), standard error ($n_{glycan-stats}$=39, $n_{motif-stats}$=86) and marginal R^2 ($n_{glycan-stats}$=21,
630 $n_{motif-stats}$=47) were used to compare model performance. Robustness measures from glycan-
631 trained and glyco-motif-trained models were compared using one-sided Wilcoxon rank sum test
632 with continuity correction. We validated these findings using a 10,000 iteration one-sided, two-
633 sample bootstrapping t-tests (Rv3.6::nonpar::boot.t.test); bootstrapping p-values were less than
634 or equal to Wilcoxon rank sum p-values within 0.001. Finally, using the Rv3.6::pwr::pwr.r.test
635 v1.2.2 package, statistical power was predicted between n=5 and n=200 for the median and
636 interquartile range of effect sizes observed in glyco-motif-trained and glycan-trained models.
637

638

639 ## Figure Legends

640 **Fig. 1 | The GlyCompare workflow for glycoprofile decomposition and comparison. a**,
641 Sixteen glycoprofiles from glycoengineered recombinant EPO cluster poorly when based solely
642 on raw glycan abundance. **b**, GlyCompare was used to compute and cluster EPO glyco-motif
643 vectors, resulting in three dominant clusters of glycoprofiles and a few individuals that have
644 severe changes in their glycan structural pattern (distance threshold=0.5) and twenty-four
645 clusters of glycan substructures (distance threshold=0.19). **c and d**, A glycoprofile with
646 annotated structure and relative abundance is obtained and the glycans are decomposed to a
647 substructure set ***S*** and the presence/absence vectors is built. Presence/absence vectors are
648 weighted by the glycan abundance, and are summed into a substructure vector ***p***. **e** , Seven
649 example glycoprofiles are represented here with their substructure vectors. **f,** To simplify the
650 substructure vectors to contain a minimal number of substructures, a substructure network is
651 constructed to identify the non-redundant glyco-motifs that change in abundance from their
652 precursor substructures. **g**, The glycoprofiles can be re-clustered with simplified glyco-motif
653 vectors for a clearer result. **h**, Clustered substructures can be analyzed to identify the most
654 representative structure in the group. For example, four substructures with different relative
655 abundance were aligned together and the monosaccharides with weight over 51% were
656 preserved.

657

658 **Fig. 2 | Changes in representative substructures can be quantified and compared to WT. a**,
659 The representative substructure table contains representative substructures for each of the 24
660 substructure clusters. The color scale represents the averaged abundances of the substructures in
661 each cluster. The substructures are sorted based on the glycan structure complexity, followed by

662 the number of branches, the degree of galactosylation, sialylation, and fucosylation. **b**, The
663 significantly differentially expressed glycan substructures are illustrated by Standard-scaled
664 abundance of twenty-four glycan substructures, compared with WT. **c**, Differential fucosylation
665 is illustrated for the Fut8 knockout. The red (black) triangles represent the presence/absence of
666 fucose in the representative substructures. Differential sialylation is illustrated for the St3gal4/6
667 knockout. The purple/black diamonds represent the presence/absence of the sialylation in the
668 representative substructures. **d**, Changes in branching are presented for the Mgat4a/4b/5
669 knockouts. The tetra-antennary substructures (Rep16 - 22) decreased considerably. The
670 triantennary substructures with elongated GlcNac (Rep13 -14) increase significantly (p-value <
671 0.0031). However, the elongated triantennary structure (Rep15) decreases considerably for the
672 Mgat5 and Mgat4b knockouts, while the Mgat4a/4b knockouts remain high abundance (p-value<
673 0.0031). In the CHO dataset, the glycan substructure generated by Mgat4a/4b and Mgat5 will be
674 considered as the same topologically.
675
676 **Fig. 3 | Analysis of intermediate substructures with GlyCompare elucidates associations in**
677 **abundance and flux with secretor status over time, which are missed in the standard whole-**
678 **glycan analysis. a**, The substructure intermediates for four connected HMOs are shown here.
679 The synthesis of larger HMOs must pass through intermediate substructures that are also
680 observed HMOs, where the substructures are as associated with measured HMOs as follow
681 X40=LNT, X62=LSTb, X106=DSLNT, X138=DSLNH. **b-e**, Over time (DPP), X62, LSTb,
682 DSLNT, and DSLNH show different trends for secretors and non-secretors. Furthermore, the
683 abundance of aggregated X62 shows significant positive-correlation with secretor and negative-
684 correlation with non-secretor. **f and g**, Panels examine the product-substrate ratio for two

685 reactions in panel **a**. X40, the LNT substructure, is a precursor to X62, the LSTb substructure,
686 which is a precursor to X106, the DSLNT substructure. We estimate the flux of these
687 conversions from X40 to X62 and X62 to X106 by examining the product-substrate ratio, i.e.,
688 the proportion of the total synthesized substrate converted to the product. LSTb/LNT
689 substructure relative abundance ratios are not associated with secretor status while DSLNT/LSTb
690 ratios are. Odds ratios (OR) corresponding the ratio association with secretor status.
691
692 **Fig. 4 | Glyco-motif level statistics require half as many samples to reach the same level of**
693 **statistical power. a and b,** The use of glyco-motifs improves measures of regression robustness.
694 The coefficient magnitude and Standard Error indicate the magnitude of the measured effect and the
695 confidence with which a coefficient can be estimated. **c**, The R^2 describes the effect size of a regression;
696 we used marginal R^2 (mR^2) because it was appropriate for the regression models used[34]. **d,** We predicted
697 power for a range of sample sizes (n=5-200) given the median effect size (solid line) within the
698 interquartile range (shaded region) for glyco-motif-trained regressions (mR^2: median=0.45, Q1=0.31,
699 Q3=0.68) and the median effect size for glycan-trained regressions (mR^2: median=0.33, Q10.18,
700 Q3=0.44). Here, the use of GlyCompare and glyco-motif abundances required approximately half the
701 number of samples to achieve equivalent power as standard glycan measures.
702

703 **Fig. 1 | GlyCompare effectively clusters panels of distinct glycoprofiles through glycoprofile**

704 **decomposition and glyco-motif identification.**

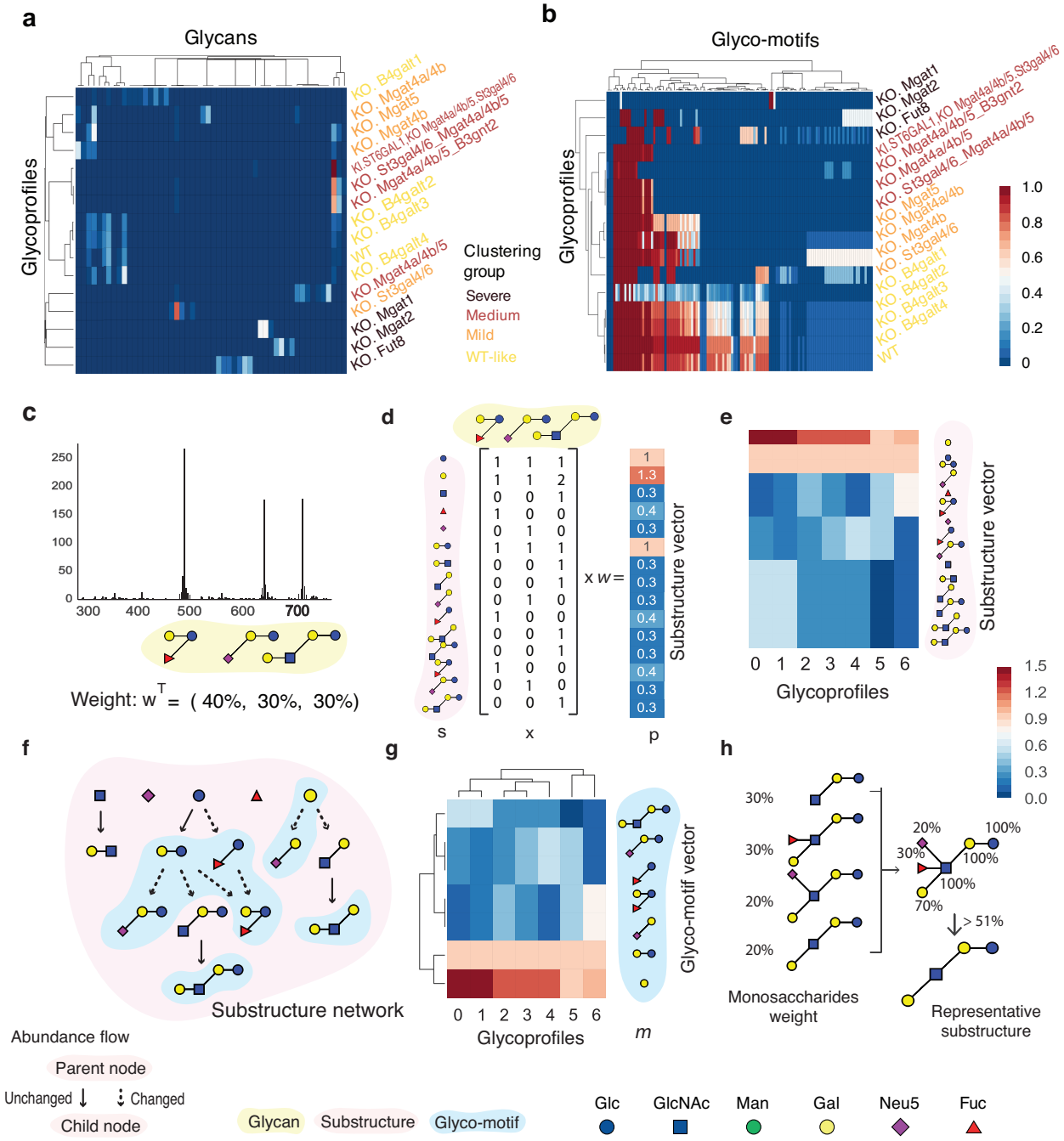

705

Fig. 2 | Changes in representative substructures can be quantified and compared to WT with the standard-scaled abundance bar plot

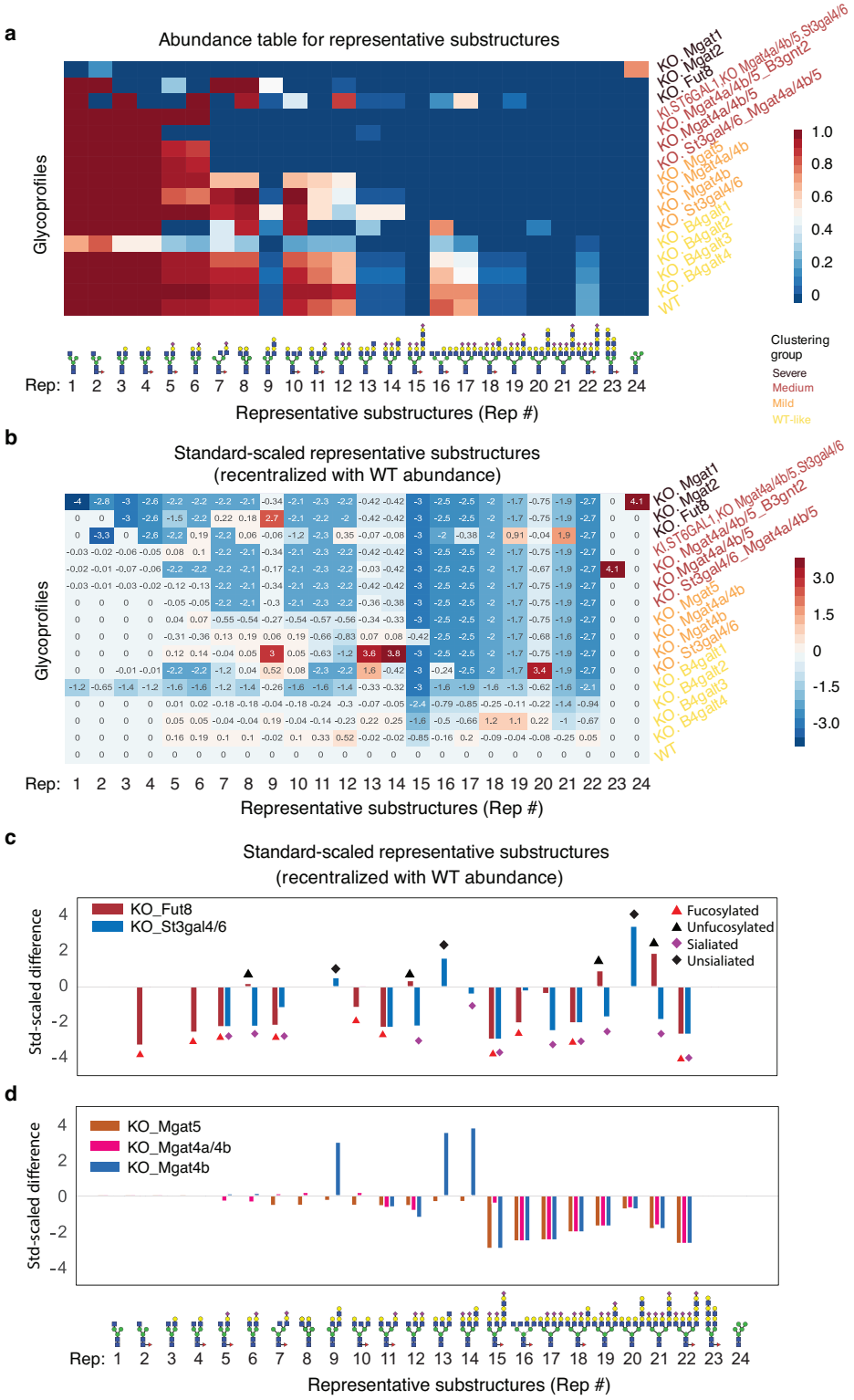

709 **Fig. 3 | Analysis of intermediate substructures with GlyCompare elucidates associations in**

710 **abundance and flux with secretor status, which are missed in the standard whole-glycan**

711 **analysis.**

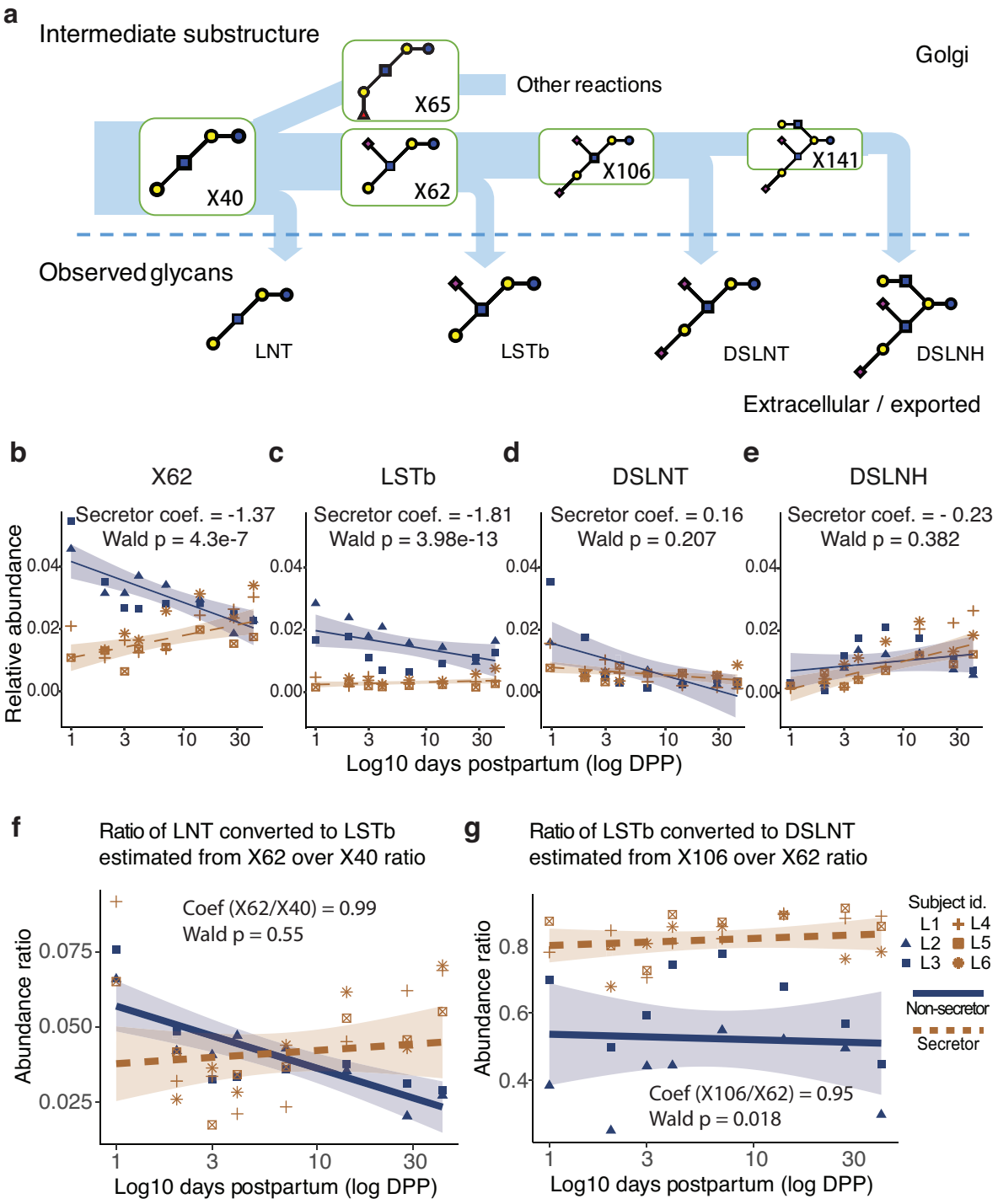

712

713 **Fig. 4 | Glyco-motif level statistics require half as many samples to reach the same level of**

714 **statistical power**

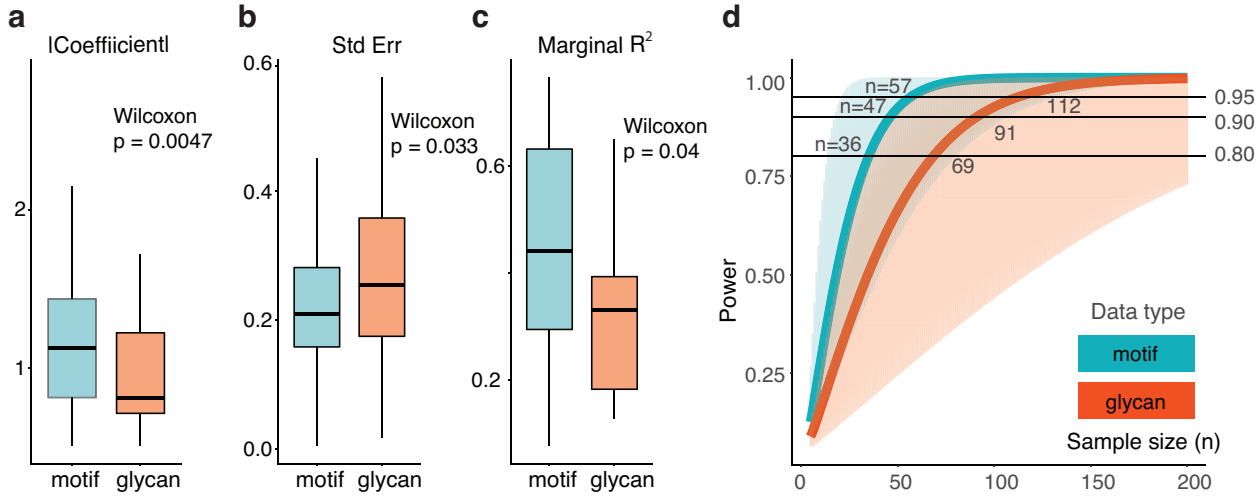

715